

Signatures of CP-violation in $\gamma\gamma \rightarrow H$ using polarized beams¹

G.J. Gounaris and G.P. Tsirigoti

Department of Theoretical Physics, University of Thessaloniki,
GR 54006, Thessaloniki, Greece

Abstract

The possibility of observing CP-violation in the process $\gamma\gamma \rightarrow H$ is investigated for masses of the Higgs particle in the interval $M_Z \lesssim m_H \lesssim 2m_t$, using a 0.5TeV tunable linear e^+e^- collider through laser backscattering. The use of polarized beams allows the formation of two different asymmetries sensitive CP-violating New Physics (NP) interactions among the gauge and Higgs bosons. It is shown that very low values of the corresponding NP couplings can be probed, for a large range of the Higgs mass.

¹Partially supported by the EC contract CHRX-CT94-0579.
Email: georgia@ccf.auth.gr

1 Introduction

High energy e^-e^+ linear colliders are crucial in thoroughly investigating the Higgs sector of the Standard Model (SM) and beyond. Their significance is twofold:

Assuming that the Higgs particle really exists and its mass is below 1TeV, it is generally believed that Higgs production at LHC or in e^-e^+ collisions, through W^+W^- fusion or $e^-e^+ \rightarrow HZ$, will give a good signal leading to the discovery of the Higgs boson [1, 2].

Once the Higgs boson is detected and its mass is measured, one would like to test whether its properties are as predicted by SM. This means measuring its width and its interactions with the matter and gauge fields. In this respect, it is necessary to check whether New Physics (NP) beyond SM exists, which induces new Higgs interactions. The e^-e^+ Linear Colliders, applied either directly or in their $\gamma\gamma$ mode, provide a very useful machinery for such studies. Since in SM the $\gamma\gamma H$ coupling arises only at the one loop level and it is mediated by loops of all charged particles with non zero mass, measurement of $\gamma\gamma \rightarrow H$ can reveal the existence of possibly new interactions induced by new heavy particles that cannot be directly produced in these next generation colliders [3].

In the present work we assume that no new particles responsible for the New Physics (NP) beyond SM, will be producible in the future colliders. Moreover, we assume that the scale Λ_{NP} of NP is sufficiently large and that the Higgs particle really exists. Under these conditions, a description of NP may be given in terms of its residual effects described in terms of *dimension* = 6 $SU(3) \times SU(2) \times U(1)$ gauge invariant operators creating new CP conserving and CP violating couplings [4]. A complete list of such operators inducing purely bosonic CP conserving couplings among the Higgs and the gauge bosons can be looked at [5, 6, 7].

On the other hand, the complete list of the *dim* = 6 purely bosonic CP-violating and $SU(3) \times SU(2) \times U(1)$ gauge invariant operators, may be represented as

$$\tilde{\mathcal{O}}_W = \frac{1}{3!} \epsilon_{ijk} W^{i\mu\nu} W_{\nu\lambda}^j \tilde{W}^{k\lambda}_{\mu} , \quad (1)$$

$$\tilde{\mathcal{O}}_G = \frac{1}{3!} f_{ijk} G^{i\mu\nu} G_{\nu\lambda}^j \tilde{G}^{k\lambda}_{\mu} , \quad (2)$$

$$\tilde{\mathcal{O}}_{WW} = (\Phi^\dagger \Phi) \mathbf{W}^{\mu\nu} \cdot \tilde{\mathbf{W}}_{\mu\nu} , \quad (3)$$

$$\tilde{\mathcal{O}}_{BB} = (\Phi^\dagger \Phi) B^{\mu\nu} \tilde{B}_{\mu\nu} , \quad (4)$$

$$\tilde{\mathcal{O}}_{GG} = (\Phi^\dagger \Phi) \delta_{ij} G^{i\mu\nu} \cdot \tilde{G}_{\mu\nu}^j . \quad (5)$$

$$\tilde{\mathcal{O}}_{BW} = \frac{1}{2} \Phi^\dagger B_{\mu\nu} \tau \cdot \tilde{\mathbf{W}}^{\mu\nu} \Phi , \quad (6)$$

where *e.g.* $\tilde{\mathbf{W}}_{\mu\nu} = \frac{1}{2} \epsilon_{\kappa\lambda\mu\nu} \mathbf{W}^{\kappa\lambda}$. This list of operators differs from the one in [8, 9] in the respect that we have included the gluonic operators $\tilde{\mathcal{O}}_G$ and $\tilde{\mathcal{O}}_{GG}$ and omitted

$$\tilde{\mathcal{O}}_{W\Phi} = i (D_\mu \Phi)^\dagger \tau \cdot \tilde{\mathbf{W}}^{\mu\nu} (D_\nu \Phi) , \quad (7)$$

$$\tilde{\mathcal{O}}_{B\Phi} = i (D_\mu \Phi)^\dagger \tilde{B}^{\mu\nu} (D_\nu \Phi) , \quad (8)$$

since they are related to the operators in (1-6) through

$$\tilde{\mathcal{O}}_{W\Phi} = \frac{g}{4} \tilde{\mathcal{O}}_{WW} + \frac{g'}{2} \tilde{\mathcal{O}}_{BW} \quad , \quad (9)$$

$$\tilde{\mathcal{O}}_{B\Phi} = \frac{g'}{4} \tilde{\mathcal{O}}_{BB} + \frac{g}{2} \tilde{\mathcal{O}}_{BW} \quad . \quad (10)$$

In (7, 8), D_ν is the usual gauge covariant derivative. Various dynamical scenarios for the arising of such operators, have been discussed in [10, 7]. Motivated from these we note in particular, that the gluonic operators $\tilde{\mathcal{O}}_G$ and $\tilde{\mathcal{O}}_{GG}$ are very easily generated if the heavy particles inducing NP are coloured.

In e^-e^+ , $\gamma\gamma$ and $e\gamma$ collisions producing gauge and/or Higgs bosons, both, the CP-conserving and the CP-violating interactions contribute [2, 11, 12]. In order to be able to disentangle the CP violating interactions, suitable processes and polarization effects must be looked at [9, 13, 14, 15]. Thus, looking at the operators presented in (1-6), we remark that the most efficient way to disentangle $\tilde{\mathcal{O}}_W$ and $\tilde{\mathcal{O}}_{BW}$ is probably through polarized $e^-e^+ \rightarrow WW$ production in the Next Linear Collider (NLC) at 500GeV and above [16]. The Higgs involving CP violating NP couplings induced by the operators $\tilde{\mathcal{O}}_{WW}$ and $\tilde{\mathcal{O}}_{BB}$ could then be disentangled by studying suitable polarization effects and angular dependencies in $e^-e^+ \rightarrow H\gamma$, HZ [8, 14, 15], as well as in $\gamma\gamma \rightarrow WW$ [17, 9], and in single Higgs production.

In this paper we study $\gamma\gamma \rightarrow H$ for suitably polarized laser and e^\pm beams and construct two asymmetries which are sensitive to CP violating Higgs gauge boson interactions. These asymmetries are analogous to those used in [9] for studying $\gamma\gamma \rightarrow WW$. It turns out that they are both sensitive to the same combination of the $\tilde{\mathcal{O}}_{WW}$ and $\tilde{\mathcal{O}}_{BB}$ couplings. The high photon luminosities expected in these machines though, combined with a reasonably expected adequate understanding of the background, guarantees that a very high sensitivity to this coupling combination, should be possible. Augmenting this information with the one obtained from $e^-e^+ \rightarrow H\gamma$, HZ , will allow a thorough study of all possible CP violating Higgs involving interactions, induced at the level of $dim = 6$ gauge invariant operators.

2 Polarization asymmetries sensitive to CP violation in $\gamma\gamma \rightarrow H$.

Polarization effects in the process $\gamma\gamma \rightarrow H$ provide a very efficient way of disentangling the operators $\tilde{\mathcal{O}}_{WW}$ and $\tilde{\mathcal{O}}_{BB}$ from the rest of the CP-conserving and the CP-violating $dim = 6$ $SU(3) \times SU(2) \times U(1)$ gauge invariant interactions; (compare (3, 4)). The effective Lagrangian describing the part of NP induced by these operators is

$$\mathcal{L}_{NP} = \frac{\bar{d}}{v^2} \tilde{\mathcal{O}}_{WW} + \frac{\bar{d}_B}{v^2} \tilde{\mathcal{O}}_{BB} \quad , \quad (11)$$

where $v = 2M_W/g \simeq 246\text{GeV}$. From this we calculate the NP contribution to the $\mathcal{T}_{\mu_1\mu_2}$ amplitude for $\gamma\gamma \rightarrow H$, where μ_1 and μ_2 are the helicities of the two incoming photons¹. We remark that CP-transformation implies for this amplitude that

$$\mathcal{T}_{\mu_1 \mu_2} = \pm \mathcal{T}_{-\mu_2 -\mu_1} , \quad (12)$$

where the upper (lower) sign is valid for the CP-conserving (CP-violating) part of the amplitude.

In Appendix A we give the density matrix \mathcal{R} (in the helicity basis), of the two colliding photons, produced by backscattering of two laser beams from the incoming highly energetic e^\pm . Using (A.19), we write

$$\sigma(\gamma\gamma \rightarrow H) = \left\{ \frac{d\mathcal{L}^{\gamma\gamma}(\tau)}{d\tau} \right\}_{\tau=\tau_H} \frac{\pi}{s_{ee}m_H^2} \sum_{\mu_j} \mathcal{T}_{\mu_1\mu_2} \mathcal{T}_{\mu_1'\mu_2'}^* \langle \rho_{\mu_1\mu_1'}^{BN} \bar{\rho}_{\mu_2\mu_2'}^{BN} \rangle , \quad (13)$$

where the $\gamma\gamma$ luminosity has been defined through (A.21, A.8, A.9), $\tau_H \equiv m_H^2/s_{ee}$, while the normalized density matrices of the two backscattered photons are given by (A.4) as

$$\begin{aligned} \rho^{BN} &= \frac{1}{2} \begin{pmatrix} 1 + \xi_2(x) & -\xi_{13}(x)e^{-2i\varphi} \\ -\xi_{13}(x)e^{+2i\varphi} & 1 - \xi_2(x) \end{pmatrix} , \\ \bar{\rho}^{BN} &= \frac{1}{2} \begin{pmatrix} 1 + \bar{\xi}_2(x) & -\bar{\xi}_{13}(x)e^{2i\bar{\varphi}} \\ -\bar{\xi}_{13}(x)e^{-2i\bar{\varphi}} & 1 - \bar{\xi}_2(x) \end{pmatrix} . \end{aligned} \quad (14)$$

In the definition of the azimuthal angle $\bar{\varphi}$ for the second photon in the last equation, the sign has been changed to take care of the fact that we choose to define it not around its own momentum, but rather around the momentum of the oppositely moving photon.

The $\gamma\gamma \rightarrow H$ cross section defined in (13) is then given as

$$\begin{aligned} \sigma(\gamma\gamma \rightarrow H) &= \left\{ \frac{d\mathcal{L}^{\gamma\gamma}(\tau)}{d\tau} \right\}_{\tau=\tau_H} \cdot \left[(1 + \langle \xi_2 \bar{\xi}_2 \rangle) \Sigma_{unp} \right. \\ &\quad \left. + \langle \xi_{13} \bar{\xi}_{13} \rangle \cos[2(\varphi - \bar{\varphi})] \Sigma_1 + \langle \xi_{13} \bar{\xi}_{13} \rangle \sin[2(\varphi - \bar{\varphi})] \Sigma_2 + \langle \xi_2 + \bar{\xi}_2 \rangle \Sigma_3 \right] , \end{aligned} \quad (15)$$

where the averages of (the products of) the ξ_j parameters, determining the density matrices of the backscattered photons, have been defined through (A.22, A.23, A.19). In (15) we have used the definitions

$$\Sigma_{unp} = \frac{\pi}{4s_{ee}m_H^2} \{ |\mathcal{T}_{++}|^2 + |\mathcal{T}_{--}|^2 \} , \quad (16)$$

$$\Sigma_1 = \frac{\pi}{2s_{ee}m_H^2} \text{Re}(\mathcal{T}_{++}\mathcal{T}_{--}^*) = \Sigma_{unp} , \quad (17)$$

$$\Sigma_2 = \frac{\pi}{2s_{ee}m_H^2} \text{Im}(\mathcal{T}_{++}\mathcal{T}_{--}^*) , \quad (18)$$

$$\Sigma_3 = \frac{\pi}{4s_{ee}m_H^2} \{ |\mathcal{T}_{++}|^2 - |\mathcal{T}_{--}|^2 \} . \quad (19)$$

¹The phase of \mathcal{T} is defined by its connection to the \mathcal{S} -matrix as $\mathcal{S} = 1 + i\mathcal{T}$.

According to (12), only Σ_2 and Σ_3 are sensitive to the CP violating NP couplings to linear order. Thus, to 1-loop order in the SM contribution, and to linear order in the CP violating NP couplings of (11), we have

$$\Sigma_{unp} = \frac{G_F m_H^2 \alpha^2}{16\sqrt{2}\pi s_{ee}} \left| \frac{4}{3}F_t + F_W \right|^2, \quad (20)$$

$$\Sigma_1 = \frac{G_F m_H^2 \alpha^2}{16\sqrt{2}\pi s_{ee}} \left| \frac{4}{3}F_t + F_W \right|^2, \quad (21)$$

$$\Sigma_2 = \frac{-G_F m_H^2 \alpha}{\sqrt{2}s_{ee}} \operatorname{Re} \left(\frac{4}{3}F_t + F_W \right) (\bar{d}s_W^2 + \bar{d}_B c_W^2), \quad (22)$$

$$\Sigma_3 = \frac{-G_F m_H^2 \alpha}{\sqrt{2}s_{ee}} \operatorname{Im} \left(\frac{4}{3}F_t + F_W \right) (\bar{d}s_W^2 + \bar{d}_B c_W^2), \quad (23)$$

where F_t and F_W , which denote the top and W loop SM contributions, can be found in [18, 3, 11].

The expected annual number of events for double laser backscattering in e^-e^+ colliders, is obtained by multiplying the cross-section in (13) with the annual luminosity $\mathcal{L}_{ee} \simeq 20fb^{-1}\text{year}^{-1}$ for a $0.5TeV$ collider. Therefore

$$N_{\tau_H} = \mathcal{L}_{ee} \sigma(\gamma\gamma \rightarrow H). \quad (24)$$

We next construct the two possible CP-odd asymmetries. The first may be observable whenever there are non-vanishing average linear polarization parameters ξ_{13} and $\bar{\xi}_{13}$ for the two colliding photons. It is obtained by performing measurements for two different values of the angle $\chi \equiv \varphi - \bar{\varphi}$ between the linear polarizations of these photons. It is given by

$$\tilde{A}_{lin} = \frac{|N_{\tau_H}(\chi = \frac{\pi}{4}) - N_{\tau_H}(\chi = -\frac{\pi}{4})|}{N_{\tau_H}(\chi = \frac{\pi}{4}) + N_{\tau_H}(\chi = -\frac{\pi}{4})} = \frac{\langle \xi_{13} \bar{\xi}_{13} \rangle}{1 + \langle \xi_2 \bar{\xi}_2 \rangle} A_{lin}, \quad (25)$$

with

$$A_{lin} = \frac{|\Sigma_2|}{\Sigma_{unp}}. \quad (26)$$

As seen from (26), A_{lin} is determined through (20, 22) solely by the CP-violating NP induced quantity Σ_2 .

The construction of the second CP violating asymmetry is possible whenever there is a non vanishing average for the sum of the circular polarizations $\langle \xi_2 + \bar{\xi}_2 \rangle$ of the two back scattered photons. This requires large average helicities for both, the laser and the e^\pm beams, (see the Appendix). Using (15) and remarking that the sign of $\langle \xi_2 + \bar{\xi}_2 \rangle$ changes whenever the signs of (P_e, P_γ) and $(\bar{P}_e, \bar{P}_\gamma)$ are simultaneously changed, we construct the asymmetry \tilde{A}_{circ} by making measurements with two opposite values of these polarization pairs. We thus get

$$\tilde{A}_{circ} = \frac{|N_{\tau_H}^{++} - N_{\tau_H}^{--}|}{N_{\tau_H}^{++} + N_{\tau_H}^{--}} = \frac{|\langle \xi_2 + \bar{\xi}_2 \rangle|}{1 + \langle \xi_2 \bar{\xi}_2 \rangle} A_{circ}, \quad (27)$$

with

$$A_{circ} = \frac{|\Sigma_3|}{\Sigma_{unp}} . \quad (28)$$

Each one of the asymmetries \tilde{A}_{lin} and \tilde{A}_{circ} is a product of two factors: The first one originates from the degree of polarization of the two photons building the collider, while the second one depends on the product of an SM 1-loop contribution and another contribution sensitive to the CP violating NP interactions. This second factor is denoted respectively by A_{lin} and A_{circ} , and satisfies $A_{lin}(SM) = A_{circ}(SM) = 0$ in the SM case. To study observability limits for the NP couplings from the use of these asymmetries, we need the expressions for the expected 1-standard deviation statistical uncertainties for each of them in the SM case. These are

$$\delta A_{lin}(SM) = \frac{|1 + \langle \xi_2 \bar{\xi}_2 \rangle|}{\sqrt{(N_{\tau_H}(\chi = \frac{\pi}{4}) + N_{\tau_H}(\chi = -\frac{\pi}{4})) \langle \xi_{13} \bar{\xi}_{13} \rangle}} , \quad (29)$$

$$\delta A_{circ}(SM) = \left| \frac{1 + \langle \xi_2 \bar{\xi}_2 \rangle}{\sqrt{(N_{\tau_H}^{++} + N_{\tau_H}^{--}) \langle \xi_2 + \bar{\xi}_2 \rangle}} \right| . \quad (30)$$

We also note from (22, 23), that both asymmetries measure the same combination $\bar{d}s_W^2 + \bar{d}Bc_W^2$ of the NP couplings.

3 Testing CP violation in $\gamma\gamma \rightarrow H$ through an e^-e^+ collider.

As explained in the Appendix, the polarized photons needed to study the CP violating contributions to $\gamma\gamma \rightarrow H$, are obtained by double laser backscattering from the e^- , e^+ beams [19, 12]. The outgoing photons are produced almost in the same direction with e^- , e^+ . All relevant formulae for the description of the Compton scattering kinematics in this framework, are collected in the Appendix. Here we only note that these are characterized by two dimensionless parameters, $x_0 = 4E\omega_0/m_e^2$ and $x = \omega/E$, where E is the energy of the electron beam, ω_0 is the laser energy and x is the fraction of the e^- beam energy carried away by the final photon. The maximum value of x is determined by x_0 , through the relation $x_{max} = x_0/(1+x_0)$. Operation of the collider below the e^-e^+ pair production threshold sets an upper limit to the value of x_0 , so that $x_0 \leq 2(1+\sqrt{2})$. Thus the final photons can take, as much as $\sim 83\%$ of the electron beam energy; compare (A.5). A lower limit in the value of x_0 is also set for each specific process under consideration, by the masses of the particles produced in the process studied [13]. Therefore, the allowed range for x_0 , for a given e^-e^+ center of mass energy is

$$\frac{\sum_{i=1}^n m_i}{\sqrt{s} - \sum_{i=1}^n m_i} \leq x_0 \leq 2(1+\sqrt{2}) , \quad (31)$$

where the sum includes all produced masses in a $\gamma\gamma$ collision.

There are various general options for operating the photon-photon collider [19, 12]:

- The conversion point (C.P.) where the Compton backscattering occurs, may be a few cm away from the interaction point (I.P.) where the $\gamma\gamma$ collisions take place. Since the most energetic photons are those with the smallest scattering angle, it is only those that finally manage to reach the I.P. Therefore, the further away from the I.P. the conversion occurs, the more monochromatic the photon beam becomes, (but with some loss in the integrated luminosity of course). This particular set up can be very advantageous for processes where production of some resonance occurs, whose mass is a priori known. In this case, the collider may be tuned, so as to operate in a narrow window around the relevant specific value of the invariant $\gamma\gamma$ mass [20, 21]. This way, there is also the possibility of reducing the background in cases where the cross-section of the main process dominates.
- Choosing a configuration where I.P. and C.P. coincide, makes the photon spectrum rather flat in the unpolarized and the $P_e P_\gamma > 0$ cases, which may be useful for searching particles with unknown masses. It may help also in the simultaneous study of more than one processes, dominating at different regions of the invariant $\gamma\gamma$ energies.

We turn now to the specific properties of the process $\gamma\gamma \rightarrow H$ in the Next Linear Collider. Assuming that the mass of the Higgs boson has been measured before, in the e^+e^- mode or perhaps at LHC, it may be possible to tune the parameters of the collider so that it operates, (to some extent), in a narrow window around the Higgs mass. The use of polarized beams in searching for any CP violating new interactions among the gauge and Higgs bosons is investigated in this section [3, 14, 22, 21]. The measurements of the two quantities A_{lin} and A_{circ} , which mostly require different polarization conditions, are considered separately.

A. Measurement of A_{lin}

As seen from (25), the measurement of A_{lin} requires laser beams with some linear polarization P_t . Then, the resulting photons building the photon-photon collider are also polarized in the same direction. The degree of linear polarization transferred to them, ξ_{13} , depends on the parameter x_0 (determining the maximum collider energy) and on P_t .

This Stokes parameter ξ_{13} is given in (A.11), as a function of its fractional energy x [19]. As explained in the Appendix and shown in Fig.3b, the degree of linear polarization ξ_{13} is very small for low energy photons, while it tends to its maximum value $\xi_{13max} = 2(1 + x_0)/[1 + (1 + x_0)^2]P_t$, when $x \rightarrow x_{max}$. It is obvious from this, that in order to increase the linear polarization transferred from the laser beams to high energy photons, it is best to have a machine design such that x_0 is as small as possible. However, when x_0 decreases, the highest Higgs mass producible through $\gamma\gamma \rightarrow H$ in a given collider, also decreases. The best choice should therefore be decided by tuning the collider after the Higgs particle discovery and the measurement of its mass.

Before discussing the actual measurement of A_{lin} , we should also mention that for the case that $m_H \lesssim 150 GeV$, in which $H \rightarrow b\bar{b}$ dominates, it may be interesting to also utilize laser beams which are partly circularly and partly linearly polarized, like *e.g.* $P_\gamma = P_t = 1/\sqrt{2}$; compare (A.1, A.2). Because then the backscattered photons acquire circular as well as linear polarizations at the same time, which should be useful for reducing the $\gamma\gamma \rightarrow b\bar{b}$ background. The reason for this is because the dependance of $\gamma\gamma \rightarrow b\bar{b}$ background on the Stokes parameters (including in particular also higher partial wave contributions), is very different from the Higgs mediated contribution given in (15).

Using therefore (partially) linear polarizations we should be able to measure the \tilde{A}_{lin} asymmetry defined in (25), which in turn determines A_{lin} and the combination $\bar{d}s_W^2 + \bar{d}_B c_W^2$ of the NP couplings; (compare (26)). To get a feeling on the possible limits that can be established, we plot in Fig.1 the ratio

$$\text{NSD for } A_{lin} \equiv \frac{A_{lin}}{\delta A_{lin}(SM)} \quad , \quad (32)$$

where (26, 29) should be used. This ratio describes number times the measurable factor A_{lin} , exceeds its expected statistical fluctuation in SM, for various choices of the NP couplings [17, 13, 9]. Fig.1 presents NSD for A_{lin} for a $\sqrt{s_{ee}} = 0.5 TeV$ collider, using the small value of $x_0 = 0.5$, as motivated above.

The sensitivity to the NP coupling combination $\bar{d}s_W^2 + \bar{d}_B c_W^2$, which can be reached by studying A_{lin} , depends on the Higgs mass. It can be obtained from Tables I and II, where the NP couplings inducing a 3σ effect are tabulated, using an integrated annual luminosity $\bar{\mathcal{L}}_{ee} \simeq 20 fb^{-1} \text{year}^{-1}$ for a 0.5TeV Collider and various values for x_0 [20]. As can be seen from these tables, the sensitivity to the above NP couplings generally increases as x_0 decreases.

The results in Table I apply for $100 \lesssim m_H \lesssim 150 GeV$ and were derived on the basis of the $H \rightarrow b\bar{b}$ mode for which a 25% detection efficiency is assumed, [20, 1, 2]. In fact, this is also what determines the overall number of the $(\varphi - \bar{\varphi})$ averaged events in the last column of the Table I. Thus, if $100 \lesssim m_H \lesssim 150 GeV$, then limits on the NP couplings $\bar{d}s_W^2 + \bar{d}_B c_W^2$ at the level $10^{-3} - 10^{-4}$ seem possible. In Table I we give results for $P_t = 1$ as well as for $P_t = 1/\sqrt{2}$ (in parentheses), in order to give a feeling of the possible implications from using laser beams with a partial circular polarization².

On the other hand, the results in Table II apply for $200 \lesssim m_H \lesssim 350 GeV$ and were derived on the basis of the $H \rightarrow ZZ \rightarrow l^- l^+ X$ mode using an efficiency of $\sim 18\%$ [20]. In both Tables I and II, it is always checked that the number of expected events for the chosen decay channels is of the order of a hundred, for all Higgs masses considered and a 0.5TeV collider.

For the high m_H part in Table II, we should also remark that as the Higgs mass increases, the sensitivity to the NP CP-violating couplings is reduced. The reason is that the lower limit for the x_0 parameter also increases and consequently the degree of linear polarization transfer decreases; (compare (31)). On top of this, there is a further

²Remember the preceding discussion concerning the $b\bar{b}$ background.

reduction of sensitivity, since A_{lin} , being proportional to the real part of SM contribution, decreases as m_H increases. However, as seen from Table II for Higgs masses in the region 200-250GeV, sensitivity limits on the NP couplings like $(\bar{d}s_W^2 + \bar{d}Bc_W^2) \sim 10^{-3} - 10^{-2}$ can be obtained at the 2σ or 3σ level, from measurements of A_{lin} .

B. Measurement of A_{circ}

Eqs. (27, A.10) indicate that the measurement of A_{circ} require the existence of circularly polarized photons, which may be obtained by backscattering similarly polarized laser beams from polarized e^\pm . Both, the energy spectrum of the resulting photons and the degree of the polarization transferred, depend on the way we choose the initial average helicities, as well as the conversion and interaction points; (see Appendix and [19, 17, 12]). If C.P. and I.P. coincide, this spectrum is rather flat for $P_e P_\gamma > 0$, and peaked towards the higher energies for $P_e P_\gamma < 0$; (compare Fig.3c).

As for the A_{lin} case, the statistical significance of a possibly non vanishing value induced by NP to A_{circ} , is again given the number of times this asymmetry exceeds the expected statistical uncertainty in SM; *i.e.*

$$\text{NSD for } A_{circ} = \frac{A_{circ}}{\delta A_{circ}(SM)} , \quad (33)$$

where (28, 30) should be used. Note that $A_{circ}(SM) = 0$.

The numerical study of (27) indicates that the measurement of A_{circ} depends very sensitively on the average polarizations along their momenta of the e^\pm beams P_e , \bar{P}_e , and of the laser photons P_γ , \bar{P}_γ . On the other hand, since the Higgs particle has no spin, in order to enhance its production we must choose the same average helicities in both arms of the collider; *i.e.* $P_e = \bar{P}_e$ and $P_\gamma = \bar{P}_\gamma$. If a configuration is selected in which the conversion and interaction points coincide, then we could choose $P_e P_\gamma = +1$, where the backscattered photons acquire for most of the energy range, a mean helicity of the same sign as the initial ones, and only very near to the maximum energy this helicity changes sign; (see Fig.3c in the Appendix). In this way the best polarization transfer is achieved (nearly 100%) for almost the entire range of the invariant $\gamma\gamma$ masses, where the luminosity is also significant.

If, however, a distance is put between C.P. and I.P., then choosing the polarizations such that $P_e P_\gamma = \bar{P}_e \bar{P}_\gamma = -1$ enhances the production of photons with the highest energies, leading thus to a gain in luminosity. Assuming that the Higgs mass is known and tuning the collider so that the most energetic photons are the ones contributing to Higgs production, allows a most efficient use of their high circular polarization which facilitates the measurement of A_{circ} . This is what is done in Fig.2a below.

It is also important observe from (28, 23), that A_{circ} is proportional to the imaginary part of the SM contribution to the $\gamma\gamma \rightarrow H$ amplitude, which is very small for $m_H \lesssim 2M_W$. This imaginary part starts becoming appreciable only above the WW -threshold. Therefore, a measurement of A_{circ} can be useful only for $m_H \gtrsim 2M_Z$, where the most useful Higgs decay mode is $H \rightarrow ZZ \rightarrow l^+ l^- X$ decay. Thus in Fig.2, we plot NSD for A_{circ} for $2M_z \lesssim m_H \lesssim 350\text{GeV}$ and various values of the NP coupling combination $\bar{d}s_W^2 + \bar{d}Bc_W^2$.

Fig.2a corresponds to $P_e P_\gamma = -1$, while Fig.2b corresponds to $P_e P_\gamma = +1$. The other parameters in these figures are chosen so that they facilitate the measurement of the A_{circ} asymmetry. Thus for the case of Fig.2a, where the spectrum of the backscattered photons is peaked towards the high energy side, we use the highest value of x_0 possible, namely $x_0 = 4.82$, as well as collider whose energy is tuned to the Higgs mass like $\sqrt{s_{ee}} = m_H/0.75$. On the contrary for Fig.2b, corresponding to a rather flat spectrum of backscattered photons, we do not tune s_{ee} to the Higgs mass, but we just fix $\sqrt{s_{ee}} = 0.5 TeV$ and $x_0 = 4$ [20]. The plots in Fig.2ab assume that C.P. and I.P. coincide.

In Tables III and IV we also give the 3σ sensitivity limits to the above couplings from A_{circ} , as a function of m_H , using the above polarization choices. In these tables we fix the energy to $\sqrt{s_{ee}} = 0.5 TeV$, and vary x_0 . It can be concluded from these Tables that sensitivity limits like $(\bar{d}s_W^2 + \bar{d}Bc_W^2) \sim 10^{-4}$, should be possible in the whole range $2M_z \lesssim m_H \lesssim 350 GeV$.

4 Final discussion

We have shown in the present work that if the Higgs particle predicted by SM really exists, then the study of the process $\gamma\gamma \rightarrow H$ using polarized beams in Next Linear Colliders, provide a very sensitive test for the existence of any CP-violating interactions among the gauge and Higgs bosons. Various polarization configurations for the e^\pm beams and the laser photons give complementary information and provide consistency checks for the study of such couplings. In particular, if the Higgs mass is in the range of (100-150)GeV, then linearly polarized laser beams may be used in a $\sim 0.5 TeV$ e^-e^+ collider, in order to measure the asymmetry \tilde{A}_{lin} defined above, which is sensitive to CP-violating NP induced interactions. This way sensitivity limits on the CP violating NP couplings at the level of $10^{-3} - 10^{-4}$ may be obtained; (compare Table I).

If the Higgs particle is in the range $2M_Z \lesssim m_H \sim 200 GeV$, then the most efficient way to look for CP violating NP interactions, is through measurement of the \tilde{A}_{circ} asymmetry, using circularly polarized beams. In this case, non vanishing average helicities for the electron as well as the laser beams are necessary, in order to have good sensitivity to the anomalous couplings. We have also seen that in case $P_e P_\gamma > 0$, it may be useful to try a tunable Linear Collider. Thus, also for these higher masses, the sensitivity limits on the NP couplings are again at the 10^{-4} level; (see Table III, IV).

In both cases, it should be possible to disentangle the CP violating forces, from the CP conserving ones affecting the same processes.

From the theoretical point of view, a nonzero value for any of these anomalous couplings provides, through unitarity, a hint on the related NP scale Λ_{NP} . Therefore, it is interesting to translate the above sensitivity limits for the couplings, to corresponding lower bounds on NP scales. Assuming that only one of the operators \tilde{O}_{WW} or \tilde{O}_{BB} acts at a time, the unitarity requirement gives the relations [15]

$$|\bar{d}| \simeq \frac{104.5(M_W/\Lambda_{NP})^2}{1 + 3(M_W/\Lambda_{NP})^2}, \quad (34)$$

$$|\bar{d}_B| \simeq \frac{195.8(M_W/\Lambda_{NP})^2}{1 + 100(M_W/\Lambda_{NP})^2} . \quad (35)$$

Using then a non vanishing value for the corresponding NP coupling at the level of the aforementioned sensitivity limits, we calculate from the unitarity relations the scale Λ_{NP} where unitarity is first reached. In general Λ_{NP} depends on the operator considered. Its value provides a rough estimate of the energy scale where either new strong interactions will develop, or new particles will be produced. From (34) and the above sensitivity limits, we would conclude that the study of $\gamma\gamma \rightarrow H$ at a $0.5TeV$ collider can probe NP scales in the range of 10-20TeV, in case NP is generated by $\tilde{\mathcal{O}}_{WW}$. Because of (35), this scale increases to 30-50TeV, if we assume that the NP forces are due to the operator $\tilde{\mathcal{O}}_{BB}$.

In summary, using polarized beams for realizing the $\gamma\gamma$ colliders, it is possible to distinguish the CP-violating NP signals from the CP conserving ones. This is not attainable if unpolarized beams are only used. The overall conclusion for the $dim = 6$ gauge invariant NP interactions considered above, is that single Higgs production in $\gamma\gamma$ collisions at $0.5TeV$ tunable linear Collider, can be used to put strong limits on the NP coupling $\bar{d}s_W^2 + \bar{d}_B c_W^2$, for Higgs masses in the ranges $100 \lesssim m_H \lesssim 150GeV$ and $200 \lesssim m_H \lesssim 350GeV$. This information is complementary and probably more precise than the one attainable through production of pairs of Higgs and/or gauge particles [23, 11, 9].

Appendix A : Density matrix of backscattered photon.

Following [19], we collect in this appendix the formulae describing the helicity density matrix of the photon produced by backscattering a laser photon from an incoming highly energetic e^\pm beam.

We denote by E the energy of the incoming e^\pm beam, while $P_e = 2\lambda_e$ describes its polarization along its momentum, and λ_e is its average helicity. The e^\pm beam is assumed to collide with a laser photon moving along the opposite direction with energy ω_0 and characterized, in the basis of its helicity states, by the normalized density matrix

$$\rho_{laser}^N = \frac{1}{2} \begin{pmatrix} 1 + P_\gamma & -P_t e^{-2i\varphi} \\ -P_t e^{+2i\varphi} & 1 - P_\gamma \end{pmatrix} . \quad (\text{A.1})$$

Here P_γ describes the average helicity of the laser photon and P_t denotes its maximum average linear polarization occurring of course along a direction perpendicular to the photon momentum, described by the azimuthal angle φ (with respect to this momentum). By definition

$$0 \leq P_\gamma^2 + P_t^2 \leq 1 . \quad (\text{A.2})$$

After the Compton scattering of e^\pm from the laser photon, the electron beam loses most of its energy and a beam of "backscattered photons" is produced, moving essentially along the direction of the original e^\pm momentum and characterized, in its helicity basis, by the density matrix

$$\rho^B = \frac{dN}{dx} \rho^{BN} , \quad (\text{A.3})$$

$$\rho^{BN} = \frac{1}{2} \begin{pmatrix} 1 + \xi_2(x) & -\xi_{13}(x) e^{-2i\varphi} \\ -\xi_{13}(x) e^{+2i\varphi} & 1 - \xi_2(x) \end{pmatrix} , \quad (\text{A.4})$$

where $x \equiv \omega/E$ and $x_0 \equiv 4E\omega_0/m_e^2$; with ω being the energy of the back-scattered photon, and ω_0 , E have been defined above. These satisfy the kinematical constraints

$$0 \leq x \leq x_{max} \equiv \frac{x_0}{1 + x_0} , \quad 0 \leq x_0 \leq 2(1 + \sqrt{2}) , \quad (\text{A.5})$$

which implies that the backscattered photon can take up to 83% of the e^\pm energy. In analogy to (A.2), the elements of ρ^{BN} also satisfy

$$0 \leq \xi_2^2(x) + \xi_{13}^2(x) \leq 1 . \quad (\text{A.6})$$

In (A.3), dN/dx is the number of backscattered photons per unit of x , normalized to a unit of flux for the incoming e^\pm beam; while ρ^{BN} is the normalized photon density matrix, ($\text{Tr} \rho^{BN} = 1$). We note from (A.4, A.1), that the azimuthal angles of the maximum average linear polarizations of the backscattered and the laser photons, defined around their respective momenta, are the same. The functions appearing in (A.3, A.4), which

determine the spectrum of the backscattered photon immediately after its production at the *conversion point*, are given by [19]

$$\frac{dN(x)}{dx} = \frac{C(x)}{D(x_0)} , \quad (\text{A.7})$$

$$C(x) = f_0(x) + P_e P_\gamma f_1(x) , \quad (\text{A.8})$$

$$D(x_0) = D_0(x_0) + P_e P_\gamma D_1(x_0) , \quad (\text{A.9})$$

$$\xi_2(x) = \frac{P_e f_2(x) + P_\gamma f_3(x)}{C(x)} , \quad (\text{A.10})$$

$$\xi_{13}(x) = \frac{2r^2 P_t}{C(x)} , \quad (\text{A.11})$$

where

$$f_0(x) = \frac{1}{1-x} + 1 - x - 4r(1-r) , \quad (\text{A.12})$$

$$f_1(x) = \frac{x}{1-x} (1-2r)(2-x) , \quad (\text{A.13})$$

$$f_2(x) = x_0 r [1 + (1-x)(1-2r)^2] , \quad (\text{A.14})$$

$$f_3(x) = (1-2r) \left(\frac{1}{1-x} + 1 - x \right) , \quad (\text{A.15})$$

$$r(x) = \frac{x}{x_0(1-x)} , \quad (\text{A.16})$$

and

$$D_0(x_0) = \int_0^{x_{max}} dx f_0(x) = \left[1 - \frac{4}{x_0} - \frac{8}{x_0^2} \right] \ln(1+x_0) + \frac{1}{2} + \frac{8}{x_0} - \frac{1}{2(1+x_0)^2} \quad (\text{A.17})$$

$$D_1(x_0) = \int_0^{x_{max}} dx f_1(x) = \left[1 + \frac{2}{x_0} \right] \ln(1+x_0) - \frac{5}{2} + \frac{1}{1+x_0} - \frac{1}{2(1+x_0)^2} , \quad (\text{A.18})$$

where x_{max} is defined in (A.5).

The elements of density matrix of the backscattered photon, for various choices of the e^\pm polarization P_e , and the laser parameters x_0 and (P_γ, P_t) , are presented in Fig.3abc. Thus, in Fig.3a, we give the backscattered photon flux dN/dx as a function of x . As seen from (A.7-A.9), dN/dx depends only on the product $P_e P_\gamma$ and the parameter x_0 determining the highest value of x through (A.5). In Fig.3b, the average linear polarization ξ_{13} of the backscattered photon is shown. As seen from comparing Fig.3ab, the demand of a high linear polarization would favour a small value of x_0 , which has the drawback that the highest energy of the back scattered photon decreases. Finally, in Fig.3c, we present the average circular polarization ξ_2 of the back scattered photon as a function of x , for various choices of P_e , P_γ and x_0 . As seen in Fig.3c, the x -dependence of ξ_2 is quite sensitive to the relative sign of P_e , P_γ .

If an e^-e^+ Collider is transformed to $\gamma\gamma$ one by using two identical lasers, then the (unnormalized) density matrix $\mathcal{R}_{\mu_1\mu_2;\mu_1'\mu_2'}$ of the $\gamma\gamma$ -pair in their helicity basis, is related

to the ρ^B , $\bar{\rho}^B$ matrices by (compare (A.3))

$$\begin{aligned} \frac{d}{d\tau} \mathcal{R}_{\mu_1\mu_2;\mu_1'\mu_2'}(\tau) &= \rho_{\mu_1\mu_1'}^B \otimes \bar{\rho}_{\mu_2\mu_2'}^B \equiv \int_{\frac{\tau}{x_{max}}}^{x_{max}} \frac{dx}{x} \rho_{\mu_1\mu_1'}^B(x) \bar{\rho}_{\mu_2\mu_2'}^B\left(\frac{\tau}{x}\right), \\ &\equiv \frac{d\mathcal{L}^{\gamma\gamma}(\tau)}{d\tau} \langle \rho_{\mu_1\mu_1'}^{BN} \bar{\rho}_{\mu_2\mu_2'}^{BN} \rangle, \end{aligned} \quad (\text{A.19})$$

where

$$\tau \equiv \frac{s_{\gamma\gamma}}{s_{ee}}, \quad (\text{A.20})$$

with s_{ee} and $s_{\gamma\gamma}$ being the squares of the c.m. energies of the e^-e^+ and $\gamma\gamma$ systems respectively. In the r.h.s. of (A.19), $d\mathcal{L}^{\gamma\gamma}/d\tau$ is the overall $\gamma\gamma$ luminosity per unit e^-e^+ flux, defined by the convolution of the separate γ luminosities appearing in (A.7-A.9). If the *conversion* points where each of the two photons are produced through laser backscattering, coincide with their *interaction* point, then

$$\frac{d\mathcal{L}^{\gamma\gamma}}{d\tau} = \frac{1}{D^2(x_0)} \int_{\frac{\tau}{x_{max}}}^{x_{max}} \frac{dx}{x} C(x) C\left(\frac{\tau}{x}\right). \quad (\text{A.21})$$

We note from (A.8, A.9), that the overall flux of the backscattered photons depends on P_e as well as on the circular polarization of the laser photons used to produce them. The definition of $d\mathcal{L}^{\gamma\gamma}/d\tau$ specifies also the definition of the "averages" $\langle \rho_{\mu_1\mu_1'}^{BN} \bar{\rho}_{\mu_2\mu_2'}^{BN} \rangle$ appearing in the r.h.s. of (A.19) for the two photons. These averages may also be used to define $\langle \xi_2 \bar{\xi}_2 \rangle$, $\langle \xi_{13} \bar{\xi}_{13} \rangle$, $\langle \xi_2 + \bar{\xi}_2 \rangle$, using the form of (A.4). Thus,

$$\langle \xi_i \bar{\xi}_j \rangle = \frac{(C\xi_i \otimes C\xi_j)}{C \otimes C}, \quad (\text{A.22})$$

$$\langle \xi_2 + \bar{\xi}_2 \rangle = \frac{(C(\xi_2 + \bar{\xi}_2) \otimes C)}{C \otimes C}. \quad (\text{A.23})$$

The above assumption that the *conversion* and *interaction* points coincide, may most probably not be imposed when the $\gamma\gamma$ collision experiments will be designed. Even in such a case though, the main modification we would need to make in the preceding formulae is to appropriately increase the lower limit in the integrals in (A.19, A.21). Thus, increasing the distance between the *conversion* and *interaction* points, will tend to select only the highest energy part of the spectrum for each of the beams of the two colliding photons.

TABLE I. 3σ upper bounds on CP-violating NP couplings from A_{lin} asymmetry, using $H \rightarrow b\bar{b}$ for the two polarization choices:
 $P_t = \bar{P}_t = 1, P_\gamma = \bar{P}_\gamma = 0, \quad (P_t = \bar{P}_t = P_\gamma = \bar{P}_\gamma = 1/\sqrt{2}, P_e = \bar{P}_e = 1).$

m_H (GeV)	x_0	upper limit on $\bar{d}_B c_W^2 + \bar{d}_S s_W^2$	$(\varphi - \bar{\varphi})$ -averaged Events
100	0.5	10^{-3} (2×10^{-3})	197 (168)
	0.8	2×10^{-2} (1.6×10^{-2})	184 (233)
	1	0.12 (0.05)	160 (255)
120	0.5	5×10^{-4} (8.5×10^{-4})	200 (160)
	0.8	8×10^{-3} (6×10^{-3})	207 (223)
	1	0.05 (0.017)	192 (264)
	1.5	0.16 (0.11)	175 (306)
140	0.5	4×10^{-4} (6.5×10^{-4})	144 (111)
	0.8	5×10^{-3} (3.2×10^{-3})	159 (143)
	1	0.03 (0.01)	156 (181)
	1.5	0.09 (0.06)	147 (237)
	2	0.22 (0.22)	138 (252)
150	0.5	5×10^{-4} (8×10^{-4})	85 (64)
	0.8	4.3×10^{-3} (3×10^{-3})	106 (87)
	1	0.023 (0.008)	107 (113)
	1.5	0.08 (0.05)	102 (157)
	2	0.2 (0.2)	97 (174)

TABLE II. 3σ upper bounds on CP-violating NP couplings from A_{lin} asymmetry, using $H \rightarrow ZZ \rightarrow l^- l^+ X$ with $P_t = \bar{P}_t = 1$, $P_\gamma = \bar{P}_\gamma = 0$.

m_H (GeV)	x_0	upper limit on $\bar{d}_B c_W^2 + \bar{d}s_W^2$	$(\varphi - \bar{\varphi})$ -averaged Events
200	0.8	10^{-3}	76
	1	1.5×10^{-3}	88
	1.5	7×10^{-3}	97
	2	0.022	102
	2.5	0.06	102
230	1	1.3×10^{-3}	51
	1.5	3.7×10^{-3}	79
	2	1.1×10^{-2}	86
	2.5	0.027	89
250	1.5	2.8×10^{-3}	66
	2	7.7×10^{-3}	72
	2.5	0.018	77
280	1.5	2.7×10^{-3}	41
	2	5.2×10^{-3}	55
	2.5	0.011	60
	4	0.074	67
300	2	4.8×10^{-3}	44
	2.5	9.3×10^{-3}	51
	4	0.055	59
330	2	1.2×10^{-2}	84
	2.5	9.8×10^{-3}	36
	4	0.044	48
	4.82	0.09	51
350	2.5	0.024	14
	4	0.06	41
	4.82	0.11	45

TABLE III. 3σ upper bounds on CP-violating NP couplings from A_{circ} asymmetry, using $H \rightarrow ZZ \rightarrow l^-l^+X$ decay and circularly polarized laser beams with $P_e = \bar{P}_e = -P_\gamma = -\bar{P}_\gamma = \pm 1$.

m_H (GeV)	x_0	upper limit on $\bar{d}_B c_W^2 + \bar{d}_S s_W^2$	ξ_2 -averaged Events
200	1	5.7×10^{-4}	141
	1.5	6×10^{-4}	133
	2	6.2×10^{-4}	121
	2.5	6.5×10^{-4}	112
	4	7×10^{-4}	95
	4.82	7.3×10^{-4}	89
240	1	6.3×10^{-4}	49
	1.5	4.2×10^{-4}	109
	2	4.3×10^{-4}	105
	2.5	4.4×10^{-4}	99
	4	4.7×10^{-4}	85
	4.82	5×10^{-4}	80
280	1.5	4.5×10^{-4}	55
	2	3.7×10^{-4}	78
	2.5	3.7×10^{-4}	78
	4	4×10^{-4}	70
	4.82	4×10^{-4}	66
320	2	4.8×10^{-4}	31
	2.5	3.6×10^{-4}	53
	4	3.5×10^{-4}	56
	4.82	3.6×10^{-4}	54
350	2.5	6×10^{-4}	15
	4	3.4×10^{-4}	45
	4.82	3.4×10^{-4}	46

TABLE IV. 3σ upper bounds on CP-violating NP couplings from A_{circ} asymmetry, using $H \rightarrow ZZ \rightarrow l^-l^+X$ decay and circularly polarized laser beams with $P_e = \bar{P}_e = P_\gamma = \bar{P}_\gamma = \pm 1$.

m_H (GeV)	x_0	upper limit on $\bar{d}_B c_W^2 + \bar{d}_S s_W^2$	ξ_2 -averaged Events
200	1	7×10^{-4}	94
	1.5	6×10^{-4}	128
	2	6×10^{-4}	131
	2.5	6.1×10^{-4}	125
	4	6.8×10^{-4}	102
	4.82	7.1×10^{-4}	92
240	1	10^{-3}	18
	1.5	5.3×10^{-4}	68
	2	4.7×10^{-4}	86
	2.5	4.6×10^{-4}	92
	4	4.7×10^{-4}	85
	4.82	5×10^{-4}	80
280	1.5	8.1×10^{-4}	17
	2	5.3×10^{-4}	39
	2.5	4.6×10^{-4}	51
	4	4.3×10^{-4}	59
	4.82	4.3×10^{-4}	58
320	2	10^{-3}	6
	2.5	6.3×10^{-4}	17
	4	4.5×10^{-4}	34
	4.82	4.4×10^{-4}	37
350	2.5	1.6×10^{-3}	2
	4	5.5×10^{-4}	18
	4.82	5×10^{-4}	22

References

- [1] Proc.Workshop on Physics at Future Accelerators, La Thuile, J.H. Mulvey, ed. CERN Report 87-07; Report, Opportunities and Requirements for Experimentation at a Very High Energy e^+e^- Collider, SLAC-329(1928); Proc. Workshops on Japan Linear Collider, KEK Reports, 90-2, 91-10 and 92-16; Physics and experiments with e^+e^- Linear Colliders, Saariselkä 1991, R. Orava, P. Eerola and M. Nordberg eds., World Scientific, Singapore 1992.
- [2] P.M. Zerwas, DESY 93-112, Aug. 1993; Proc. of the Workshop on e^+e^- Collisions at 500 GeV: The Physics Potential, DESY 92-123A,B,(1992), C(1993), D(1994), ed. P. Zerwas.
- [3] J.F. Gunion, H.E. Haber, G. Kane and S. Dawson, Higgs Hunter's Guide, (Addison-Wesley, Redwood, CA, 1990); J.F. Gunion, H.E. Haber, Phys. Rev. **D48** (1993) 5109; B. Grzadkowski and J.F. Gunion, Phys. Lett. **B294** (1992) 361.
- [4] W. Buchmüller and D. Wyler, Nucl. Phys. **B268** (1986) 621; C.J.C. Burgess and H.J. Schnitzer, Nucl. Phys. **B228** (1983) 454; C.N. Leung, S.T. Love and S. Rao Z. f. Phys. **C31** (1986) 433.
- [5] K. Hagiwara, S. Ishihara, R. Szalapski and D. Zeppenfeld, Phys. Lett. **B283** (1992) 353, Phys. Rev. **D48** (1993) 2182.
- [6] A. De Rújula, M.B. Gavela, P. Hernandez and E. Masso, Nucl. Phys. **B384** (1992) 3.
- [7] G.J. Gounaris, D.T. Papadamou and F.M. Renard, hep-ph/9609437, to appear in Z.f. Physik.
- [8] K. Hagiwara and M.L. Stong Z. f. Phys. **C92** (1994) 99.
- [9] S.Y. Choi, K. Hagiwara and M.S. Baek, Phys. Rev. **D54** (1996) 6703.
- [10] G.J. Gounaris, F.M. Renard and G. Tsirigoti, Phys. Lett. **B338** (1994) 51; Phys. Lett. **B350** (1995) 212; C. Arzt, M.B. Einhorn and J. Wudka, Nucl. Phys. **B433** (1995) 41; G.J. Gounaris, D.T. Papadamou and F.M. Renard, PM/96-31, THES-TP 96/10, hep-ph/9611224, (unpublished).
- [11] G.J. Gounaris and F.M. Renard, Z. f. Phys. **C69** (1996) 513. G.J. Gounaris, J. Layssac and F.M. Renard, Z. f. Phys. **C65** (1995) 254, **C67**1995542.
- [12] M. Baillargeon, G. Bélanger and F. Boudjema, hep-ph/9405359, Proc. "two Photon Physics from DAFNE to LEP200 and beyond", p.267, Paris February 1994.
- [13] S.Y. Choi and K. Hagiwara, Phys. Lett. **B359** (1995) 369.
- [14] M. Krämer, J. Kühn, M.L. Stong and P.M. Zerwas; Z. f. Phys. **C64** (1994) 21.

- [15] G.J. Gounaris, F.M. Renard and N.D. Vlachos, Nucl. Phys. **B459** (1996) 51.
- [16] G.J. Gounaris and C.G. Papadopoulos hep-ph/9612378.
- [17] G. Belanger and G. Couture, Phys. Rev. **D49** (1994) 5720.
- [18] L. Bergström and G. Hulth, Nucl. Phys. **B259** (1985) 137; J. Gunion, H. Haber, G. Kane and S. Dawson, The Higgs Hunter's guide, Addison-Wesley, Reading 1990; B.A. Kniehl, Phys. Rep. **C240** (1994) 211.
- [19] I.F. Ginzburg, G.L. Kotkin, V.G. Serbo and V.I. Telnov, Nucl. Instr. and Meth. **205**, (1983) 47; I.F. Ginzburg, G.L. Kotkin, V.G. Serbo, S.L. Panfil and V.I. Telnov, Nucl. Instr. and Meth. **219**, (1984) 5; V.B. Berestecky, E.M. Lifshitz and L.P. Pitaevsky, Quantum Electrodynamics (Moscow, 1980)
- [20] F. Richard, Proc. of the Workshop on e^+e^- Collisions at 500GeV : The Physics Potential, DESY 92-123A+B+C(1992), ed. P. Zerwas.
- [21] M. Baillargeon, G. Bélanger and F. Boudjema, hep-ph/9409263, Phys. Rev. **D51** (1995) 4712.
- [22] V. Barger, K. Cheung, A. Djouadi, B. A. Kniehl and P.M. Zerwas, Phys. Rev. **D49** 79.
- [23] K. Hagiwara, R. Szalapski and D. Zeppenfeld, Phys. Lett. **B318** (1993) 155.

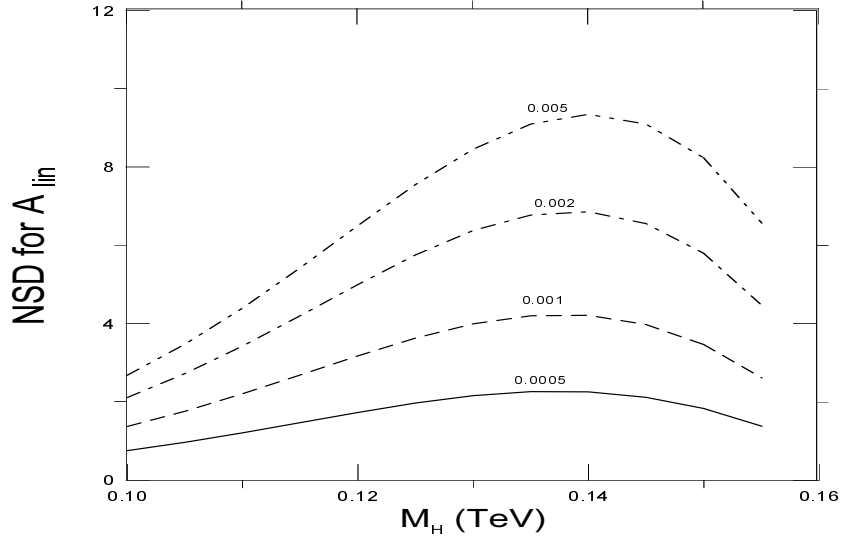
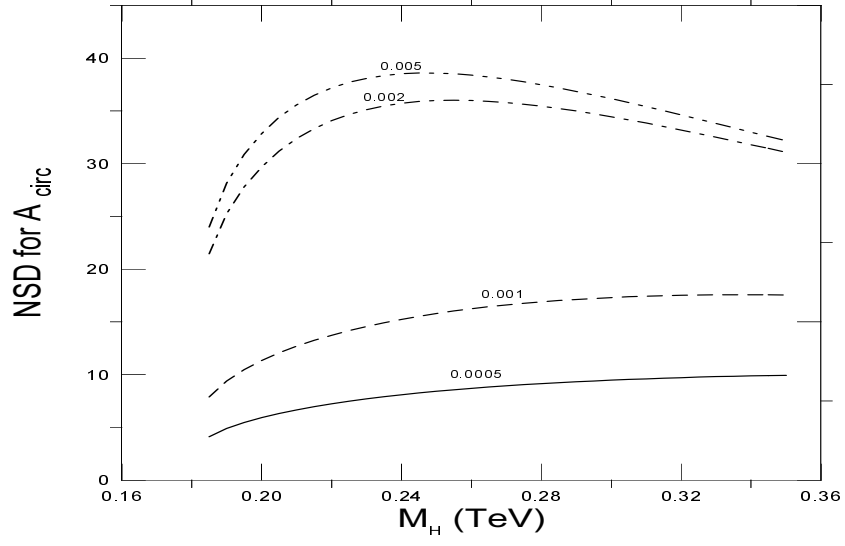
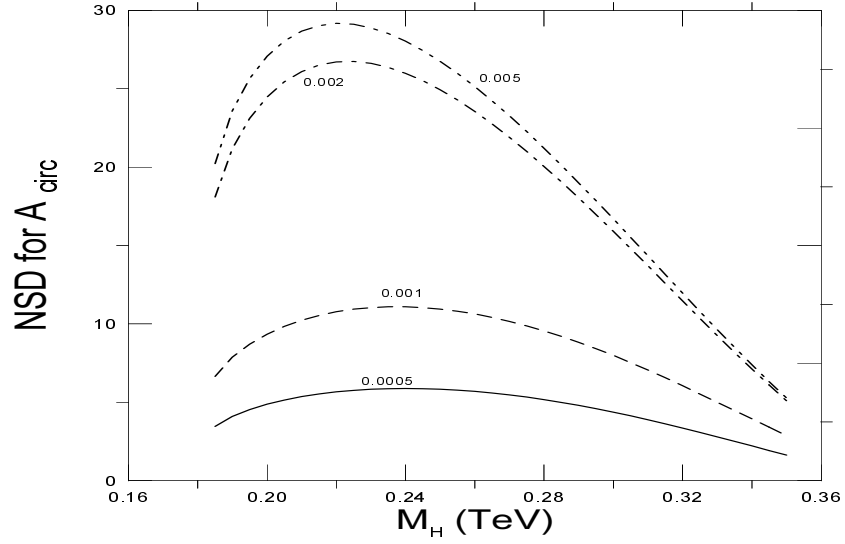


Figure 1: NSD for the A_{lin} -asymmetry, for various choices of the $(\bar{d}_B c_W^2 + \bar{d}_s s_W^2)$ combination of couplings, using $P_t = 1$ and $x_0 = 0.5$ in a $\sqrt{s}_{ee} = 0.5 TeV$ Collider.



(a)



(b)

Figure 2: NSD for the A_{circ} -asymmetry, for various choices of the $(\bar{d}_B c_W^2 + \bar{d}_S s_W^2)$ combination using: (a) $P_e = \bar{P}_e = -P_\gamma = -\bar{P}_\gamma = \pm 1$, $x_0 = 4.82$ and $\sqrt{s_{ee}} = m_H/0.75$; (b) $P_e = \bar{P}_e = P_\gamma = \bar{P}_\gamma = \pm 1$, $x_0 = 4$ and $\sqrt{s_{ee}} = 0.5 \text{ TeV}$.

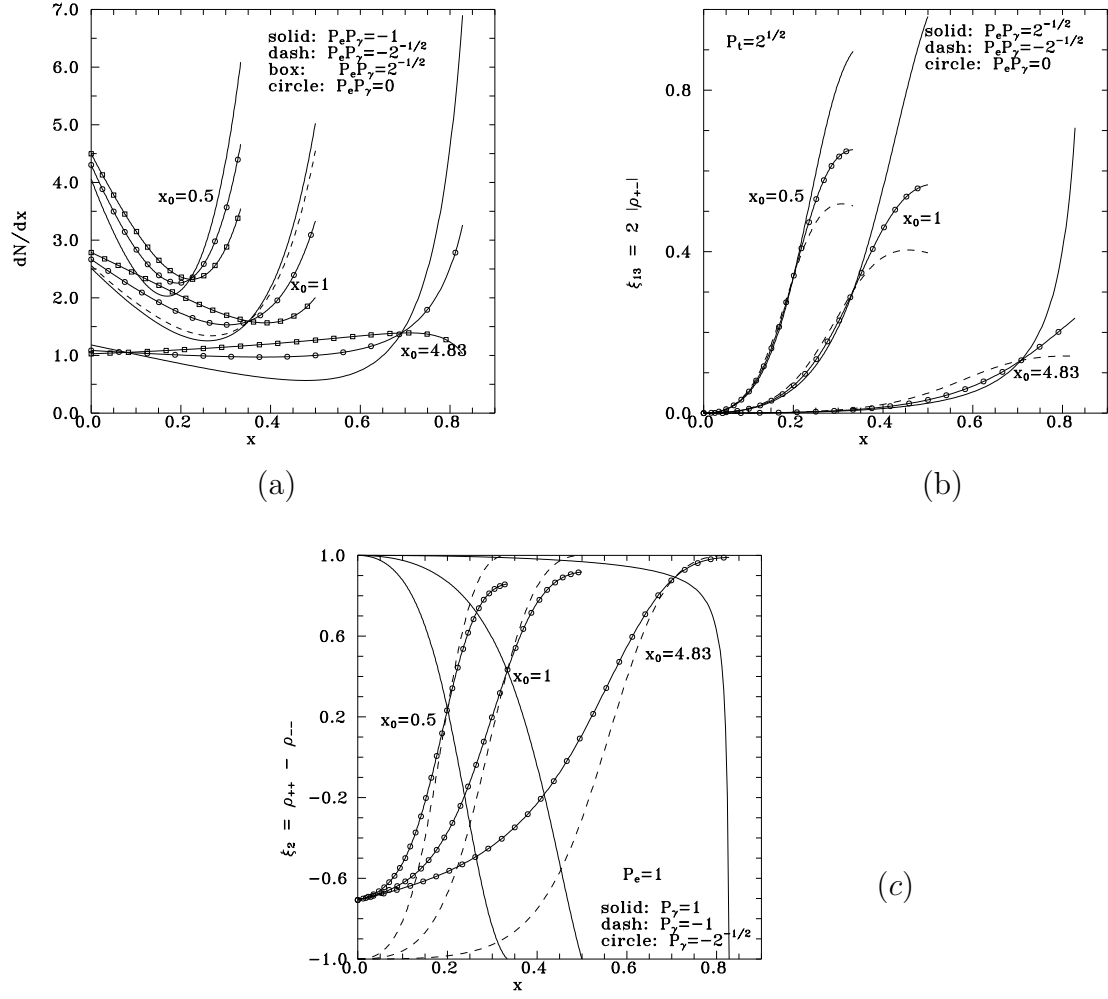


Figure 3: The spectrum of the backscattered photon; (a) overall flux, (b) average linear polarization of the backscattered photon along the direction it is maximized, and (c) average circular polarization.